LESSONS LEARNED FROM PSIC4: IMPROVING PSI RESULTS FOR A CONSTRAINED TEST SITE

Sami Samiei Esfahany, Freek J. van Leijen, Petar Marinkovic, Gini Ketelaar, and Ramon F. Hanssen

Delft Institute of Earth Observation and Space Systems,
Delft University of Technology , Kluyverweg 1, 2629 HS Delft, The Netherlands.
Email: S.Samieiesfahany@student.tudelft.nl

ABSTRACT

In the PSIC4 experiment, eight different processing approaches for time series analysis of InSAR data were applied to a data set containing an unknown deformation signal. Results of the experiment showed different spatial point density for different processing approaches. The results of most of the groups that participated in the project suffer from a low spatial density of persistent scatterers in deforming areas. This lack of PS points in the area of interest raises the hypothesis of type-I errors (falsely rejected PS) due to imperfections in the mathematical model of PS processing. We investigate the contribution of three different sources of type-I errors: atmospheric phase screen (APS) and orbital errors, non-linear deformation mechanisms, and azimuthal sub-pixel position of the scatterers. We investigate these type-I errors and present significant improvements in their identification by optimization of the mathematical model, leading to an improved density of persistent scatterers.

Key words: Persistent Scatterer; deformation; InSAR.

1. INTRODUCTION

In the PSIC4 experiment (Racoules et al., 2006), eight different processing approaches for time series analysis of InSAR data were applied to a data set containing an unknown deformation signal. The experiment proved to be highly successful, as it clearly indicated that different approaches resulted in different results, in terms of spatial point density, temporal deformation behavior, phase ambiguity resolution, and precision and reliability. Results showed a trade-off between one or more of the above characteristics, and a high sensitivity to chosen threshold values. As PSIC4 was a blind experiment, where no a-priori information on the location, magnitude, temporal behavior, and other characteristics of the deformation was available, it raises the question to what extent a-priori information can and should be used in PSI processing. Information, or assumptions, either on temporal or spatial behavior appear to be very important in the processing results.

At TU Delft, the results of the PSIC4 study have been used to evaluate algorithm performance and assess which approaches are most important to retrieve reliable deformation parameters at a high spatial density. This includes an analysis of type-I errors (falsely rejected PS) due to imperfections in the functional model (e.g., imperfection due to highly non-linear deformation, sub-pixel position of the scatterer), or in the stochastic model (e.g. imperfection due to atmospheric errors, orbit errors, geometrical decorrelation).

In this paper, we investigate the contribution of three different sources of type I errors (functionally and stochastically). We optimized the mathematical model to cope with these three sources of errors in order to decrease the false rejection rate of scatterers. The improvements are based on the Gauss-Markov model (which is used in the integer least-square and bootstrapping technique), which allows for the addition of extra parameters in the functional model and for the adoption of the stochastic model without an increase of the computational effort.

2. MATHEMATICAL FRAMEWORK

The basic concept of our PS processing approach is based on the mathematical model which can be formulated as:

$$\begin{aligned} E\{y\} &= Aa + Bb \\ D\{y\} &= Q_y, \end{aligned} \tag{1}$$

where $E\{.\}$ is the expectation operator, $D\{.\}$ the dispersion, y the vector of observations, A and B are design matrices for the integer and real valued parameter vectors a and b respectively, and Q_y is the covariance matrix.

This mathematical model comprises of the functional and the stochastic model. The functional model describes the relation between the observations and the unknowns, whereas the stochastic model represents the stochastic properties of the observations.

The functional model for a single master stack, where the master is indicated by a zero and N slave acquisitions are

available, has the form

$$E\{\begin{bmatrix} \psi^{01} \\ \vdots \\ \psi^{0N} \\ S^* \\ H^* \\ D_1^* \\ \vdots \\ D_P^* \end{bmatrix}\} = \begin{bmatrix} -2\pi & & \\ & \ddots & \\ & & -2\pi \\ & & \\ & & \\ & & \\ & & \\ & & \end{bmatrix} \begin{bmatrix} a^{01} \\ \vdots \\ a^{0N} \end{bmatrix}$$

$$+ \begin{bmatrix} \frac{-4\pi}{\lambda} & \beta^{01} & \alpha_1(t^{01}) & \dots & \alpha_P(t^{01}) \\ \vdots & \vdots & \vdots & \ddots & \vdots \\ \frac{-4\pi}{\lambda} & \beta^{0N} & \alpha_1(t^{0N}) & \dots & \alpha_P(t^{0N}) \\ 1 & & & & \\ & 1 & & & \\ & & 1 & & \\ & & & \ddots & \\ & & & & 1 \end{bmatrix} \begin{bmatrix} S \\ H \\ D_1 \\ \vdots \\ D_P \end{bmatrix}, \quad (2)$$

where ψ are the phase observations, S is the atmospheric delay of the master acquisition, H the height, D_p are deformation parameters with $p = 1 \dots P$, λ is the radar wavelength, β is the height-to-phase conversion factor, α_p describes a deformation model as function of temporal baseline t and $(.)^*$ denotes a pseudo-observable needed to solve for the rank deficiency of the system (Kampes and Hanssen, 2004). The rank deficiency is caused by the fact that for each observed phase an ambiguity needs to be estimated, together with the parameters of interest. As a result, the number of unknowns exceeds the number of observations. With the introduction of pseudo-observables, the mathematical model is regularized. Without a-priori knowledge of the topography and deformation in the area, the pseudo-observations are set to zero. To reduce the influence of atmospheric delays and orbit errors on the estimation process, differential phases between two neighboring PS candidates are used as observations. After unwrapping these *arcs* in time, a spatial testing and unwrapping algorithm is applied to obtain estimates with respect to a single reference. Additional parameters can easily be added to the functional model, e.g. sub-pixel position in azimuth direction to account for Doppler variations in the acquisitions (Kampes, 2005).

The second part of the mathematical model is the stochastic model, represented by the covariance matrix

$$D\{\begin{bmatrix} \psi \\ y^* \end{bmatrix}\} = \begin{bmatrix} Q_\psi & 0 \\ 0 & Q_{y^*} \end{bmatrix}, \quad (3)$$

where y^* represents the vector of pseudo-observations. The covariance matrix of the phase observations Q_ψ is obtained by variance component estimation (VCE) (Teunissen and Amiri-Simkooei, 2006; Kampes, 2005). The VCE technique estimates the covariance matrix directly from the data. Hence, the covariance matrix used in the estimation process is not dependent on a-priori assumptions on the quality of the data. After estimation and subtraction of certain signals, e.g. the atmospheric delay, the VCE algorithm is applied again to update the covariance matrix. The covariance matrix of the pseudo-observations Q_{y^*} contains variances which bound the solution space of the unknowns.

Using least-square estimation with the functional model, Eq. (2), and the stochastic model, Eq. (3), each phase double difference between two PS candidates is unwrapped in time. The testing criterion for accepting a scatterer as a PS is the a-posteriori variance factor

$$\hat{\sigma}^2 = \frac{e^T Q_\psi^{-1} e}{r}, \quad (4)$$

where e is the vector of residuals between the unwrapped phase and the deformation model and r is the redundancy in the functional model. A PS candidate is accepted as a PS when $\hat{\sigma}^2$ is smaller than 1.0.

3. SOURCES OF TYPE I ERRORS

Any imperfection in the functional model (e.g., imperfection due to non-linear deformation, sub-pixel position of the scatterer) results in larger deviations between observations and model. As a consequence, these large residues will result in larger $\hat{\sigma}^2$ and type-I errors, so the scatterer will be discarded for further analysis. In order to optimize the mathematical model to handle these kinds of deficiencies, an extended model with additional parameters should be used. Using extended functional models, the number of detected PS can be enlarged, albeit at the expense of decreased rank of the estimation problem. This decreased rank increases the chance on undetected unwrapping errors, denoted as type-II errors. Therefore, extended deformation models should only be applied when necessary.

On the other hand, imperfections in the stochastic model (Q_ψ) can also cause type I errors. Using a too optimistic stochastic model results in a larger $\hat{\sigma}^2$, leading to the false rejection of a PS. For example, imperfections in the stochastic model can be due to atmospheric errors, orbit errors, geometrical decorrelation or sub-pixel position of the scatterer. In general, there are two approaches to cope with these kinds of imperfections: 1) adapt the covariance matrix (adding additional values in entries of Q_ψ), or 2) remove the corresponding errors from the observations (filtering).

In this study we will investigate three sources of type-I errors: 1) APS and orbit errors 2) Non-linear deformation model and 3) Azimuthal sub-pixel position of the scatterer. We optimize the functional and the stochastic models in order to cope with these three sources of false rejections.

4. APS INTERPOLATION AND ORBIT ERRORS

In the standard PS-InSAR methodology, the residual signal of all differential arcs in the initial network is filtered

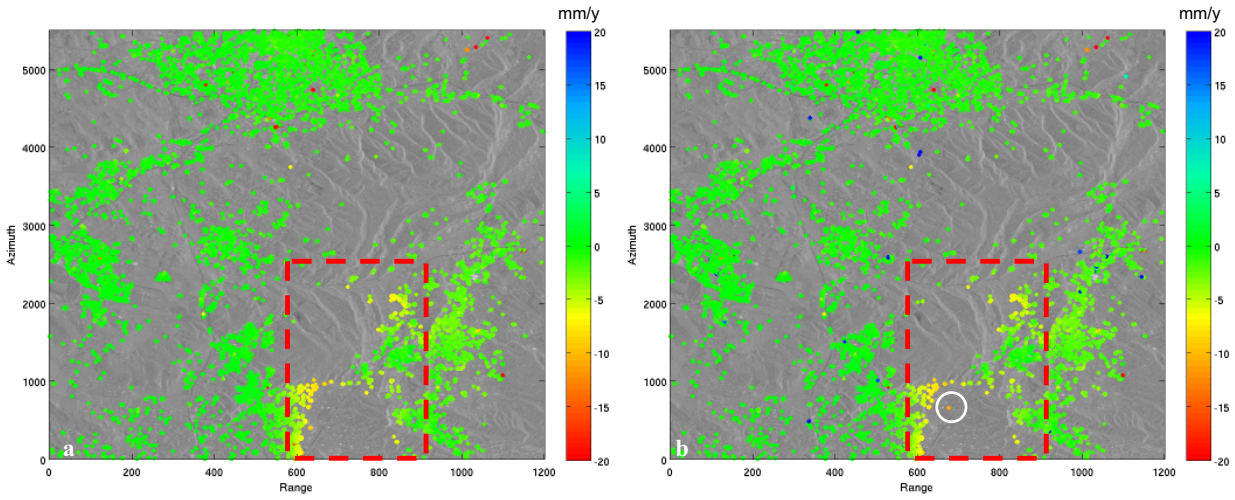

Figure 1. a) PSI results from standard PS processing using only kriging interpolation for the mining area in Gardanne, France (red dashed rectangle). b) PSI result obtained by applying adapted APS estimation with trend and stratification. Linear deformation rates estimated from the unwrapped time series are shown.

to extract the atmospheric signal per acquisition, see e.g. Ferretti et al. (2001). Based on the correlation of the atmosphere in space and its decorrelation in time, a combined smoothing and interpolation operation using kriging is used to derive the APS (i.e., the atmosphere signal for the whole scene). After subtraction of the APS from the original differential phase, the estimation procedure can be repeated for all pixels. This approach is optimal for interpolation of the turbulence signal of the atmosphere. However filtered residuals not only contain the turbulence signal but also orbit errors and vertical stratification signal of the atmosphere, see Hanssen (2001). Although differential phases between two neighboring PS candidates are used as observations in the mathematical model to reduce orbit error and stratification, these effects can be a source of error in the final estimation and cause PS to be falsely rejected especially in areas with low signal to noise ratio (e.g. non-urban areas with high non-linear deformation mechanism). Based on this hypothesis we optimized our APS interpolation approach. Instead of only using a kriging interpolation on filtered residuals, we used three steps.

1. For each acquisition, detrend the data by fitting a first order plane to the unwrapped phase and subtract the estimated trend from the original phase.
2. Estimate vertical atmospheric stratification based on the linear correlation between topography (DEM) and stratification signal and subtract it from the detrended phase.
3. Interpolate turbulence using kriging on residuals (as in standard approach).

Consequently, the final estimated APS is a summation of a trend signal, stratification, and turbulence. Fig. 1a shows the detected PS and their displacement rates obtained from standard processing using only kriging interpolation. Fig. 1b visualizes the results after applying detrending and estimation of stratification. The number of detected PS in deforming area (red dash rectangle) increased in this case from 1749 applying the standard approach to 1889 (8% improvement) using detrending and to 1911 (9% improvement) using detrending and stratification estimation. Also some PS are detected close to the center of subsidence region (white circle in Fig. 1b).

5. NON-LINEAR DEFORMATION MODEL

Because the a-posteriori variance factor $\hat{\sigma}^2$ is dependent on the deviation between the observations and the assumed deformation model (usually a linear model), large residues due to higher order deformation mechanism can result in type I errors. In other words, persistent scatterers with more complex displacement histories will not be detected. van Leijen and Hanssen (2007b,a) presented two strategies to increase the number of detected persistent scatterers using adaptive deformation models.

The first strategy is based on alternative hypothesis testing during the PSI processing. A sequential scheme is used to apply and test extended deformation models per phase double difference, intending to find a model that sufficiently fits to the data to avoid type-I errors. The adaption of the deformation model is based on hypothesis testing. The algorithm is initialized with the selection of a set of these models. Then, each phase double difference between two PS candidates is unwrapped in time applying the sequential scheme of alternative hypothesis testing until a deformation model fits to the data well enough. A linear model is a good null hypothesis because of the maximum redundancy in the estimation process. Apply-

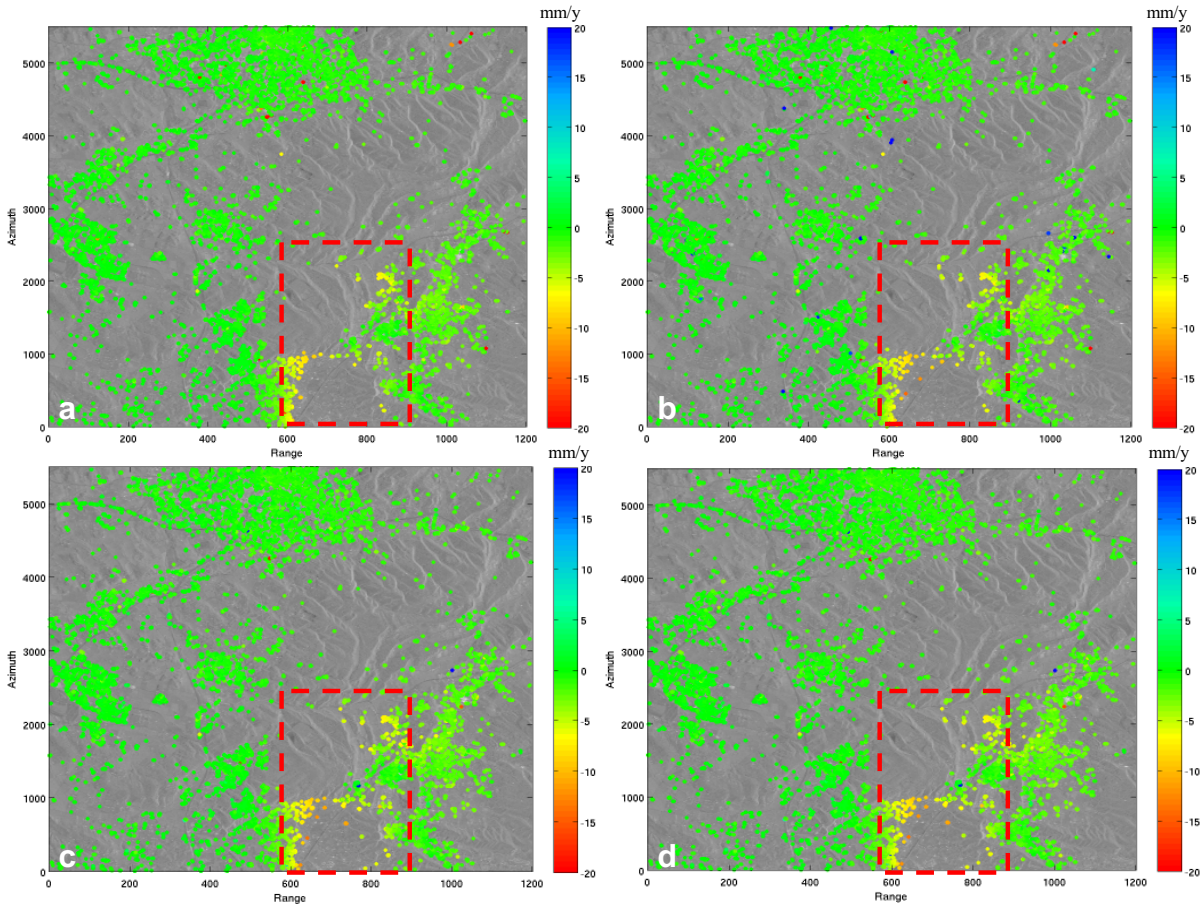

Figure 2. a) PSI result using a linear deformation model for the mining area in Gardanne, France (red dash rectangle). b) Results obtained by applying the sequential hypothesis testing scheme using a linear and a breakpoint model. The breakpoint was set a-priori at 19 May 1995. c) Result obtained by applying the sequential hypothesis testing scheme using a linear and a quadratic model. d) Result obtained using integration of the sequential hypothesis testing scheme and iterative deformation modeling using kriging. Linear deformation rates estimated from the unwrapped time series are shown.

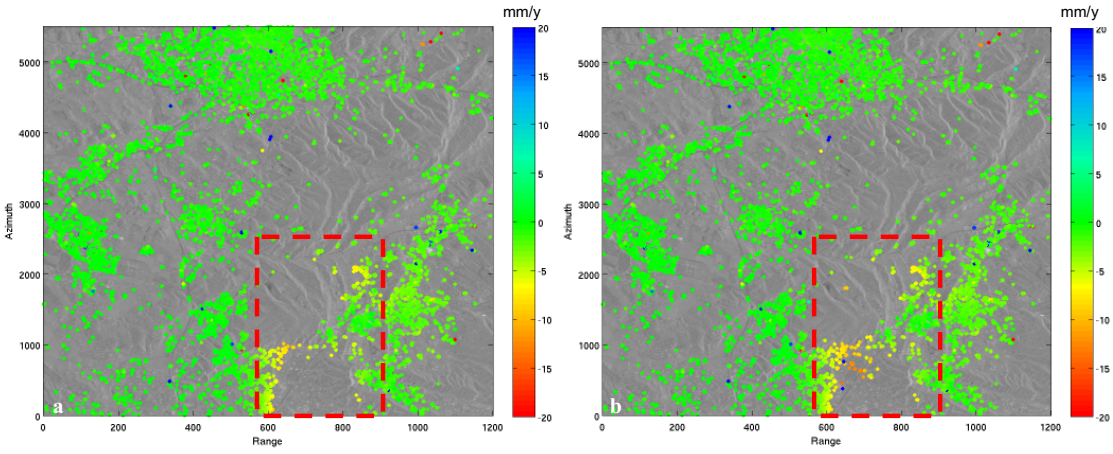

Figure 3. a) PSI result from standard PS processing using adapted functional model with azimuthal sub-pixel position for mining area in Gardanne, France (red dash rectangle). b) PSI result obtained by applying adopted stochastic model for azimuthal sub-pixel position. Linear deformation rates estimated from the unwrapped time series are shown.

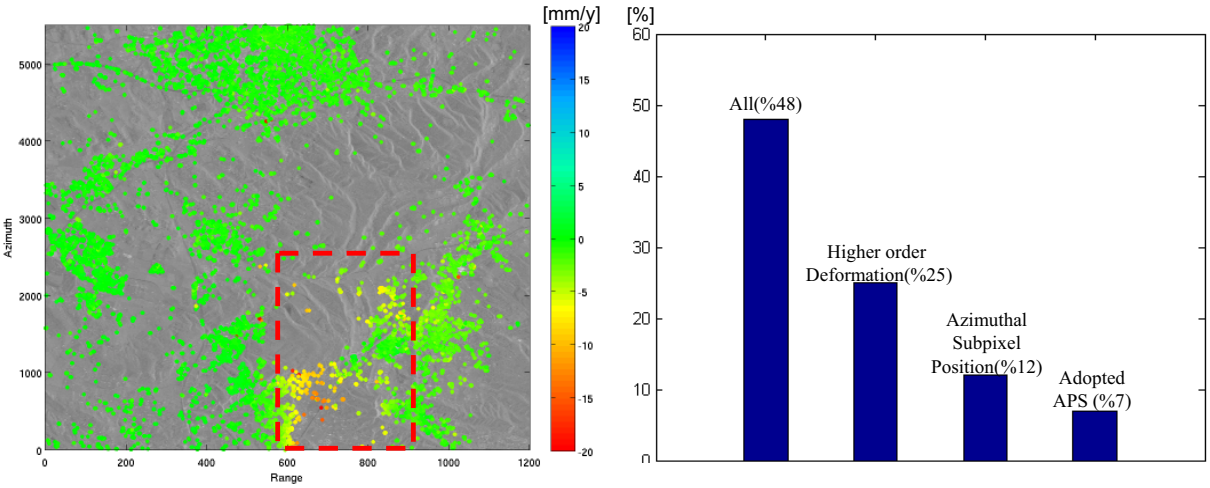

Figure 4. a) PSI result from adapted mathematical model to optimized APS interpolation, non-linear deformation, and azimuthal sub-pixel position for mining area in Gardanne, France (red dash rectangle). b) Contribution of different adaptations in the PS processing. Note that the sum of the three contribution (44%) is not equal to the total improvement (48%) due to the synergy effect.

ing the sequential scheme of hypothesis testing, a certain deformation model is accepted when $\hat{\sigma}^2$ is smaller than 1.0. Otherwise, the next model is tested until the complete set of models is evaluated.

The second method is based on an iterative scheme of deformation modeling. After a standard PSI processing under the null hypothesis, that is, applying a linear model, a deformation model is estimated based on interpolation (e.g., kriging) from the PS results. The modeled deformation is then subtracted from the original interferometric phase and the PSI processing is repeated (again using a linear model). Because the deformation models are estimated per epoch using the displacement time series, possible non-linear deformation is modeled as well. As a result, points which were previously rejected as a PS due to too large deviations from the model may now be accepted. Hereby the density of PS improves. Obviously, this procedure can be repeated iteratively. Note that a similar procedure is often followed in standard PSI processing to remove atmospheric delays and, based on auxiliary data, heights.

The results of standard processing using a linear deformation model are shown in Fig. 2a. Fig. 2b shows the result after applying the sequential testing scheme using a linear and a breakpoint model. The breakpoint model is characterized by two subsequent linear models separated by an event or breakpoint. In this study, the breakpoint is defined a-priori on 19 May 1995, based on the start of the mining activities. With this model PS are detected in the center of the subsidence region. To enable visualization, the figure shows linear deformation rates estimated through the unwrapped time series, even when the breakpoint model was used for the unwrapping. The number of detected PS in the deforming area (red dashed rectangle) increased in this case from 1749 using the linear model to 2069 (18% improvement). Fig. 2c shows the result of the sequential testing scheme using a linear and a quadratic deformation model. In this case, the number of detected PS in the area of interest increased 1749 to 2116 (20% improvement). Applying iterative deformation modeling using kriging interpolation in combination with sequential hypothesis testing (with linear, breakpoint, and quadratic deformation model) gave the results which is presented in Fig. 2d. The number of detected PS increased from 1749 to 2155 (23% improvement), confirming the expected increase in PS density. Importantly, this adaptive approach enabled the detection of a PS in the center of subsidence region.

6. AZIMUTHAL SUB-PIXEL POSITION

The sub-pixel position of a PS point in azimuth direction induces an additional phase component in the PSI observation, especially when there is a large difference between the Doppler centroid frequency of the master and slave image. This term is only important for point scatterers, since for distributed scatterers the effective phase center is approximately at center for all pixels. The azimuthal sub-pixel position can be estimated as an additional parameter in the mathematical model based on the linear relationship with the Doppler difference between the master and slave image (Kampes, 2005; Marinkovic et al., 2008)

$$\psi^{0n} = \frac{4\pi}{v}\Delta f_{dc}^{0n}.\xi_x, \tag{5}$$

where v is the satellite velocity, Δf_{dc}^{0n} is the Doppler centroid difference between master and nth acquisition, and ξ_x is the sub-pixel position of the PS in azimuth detection. However, adding this additional parameter to the functional model leads to a decreased rank of the estimation

problem. Moreover, the azimuth sub-pixel position cannot be estimated with high precision in the case of small variation of the Doppler frequencies. This suggests treating this parameter stochastically rather than functionally. That is, instead of estimating this parameter as a new unknown, introduce it in the stochastic model. That is, add extra values to the diagonal elements of the Q_{ψ}. This extra value is scaled relative to the Doppler difference of each interferogram. So observations with higher Doppler difference have higher variance and so lower weight in the estimation, leading to smaller $\hat{\sigma}^2$ and so acceptance of the PS.

However, both of these adaptions (i.e. adopt functional model or stochastic model) should be applied only when it is necessary. Estimation of the azimuthal sub-pixel position as an extra parameter for all pixels causes that pixels with small azimuthal sub-pixel position are unwrapped with an unnecessary complex model, increasing the chance of unwrapping errors (type-II errors). On the other hand, adding this term to the stochastic model for all pixels results in underestimation of $\hat{\sigma}^2$, leading to the false detection of PS (again type-II errors). So both adaptions should only be used for pixels with large azimuthal sub-pixel position. In order to detect these pixels, we analyzed the residuals (deviation between the observations and the model) after temporal unwrapping. Looking at the correlation between residuals and Doppler differences, we can detect the pixels which show high correlation with Doppler differences. Fig. 5 shows the histogram of this correlation in a small area in the Gardanne area. It is clear that these pixels can be classified in two groups: 1) a normal distribution part which contains pixels with small azimuthal sub-pixel position and also distributed scatterers with zero mean correlation with Doppler differences (red normal bell shape), and 2) pixels outside the normal bell shape which show correlation with Doppler differences (red circle). The second group contains pixels which we detected for adaption of the mathematical model for azimuthal sub-pixel position. 83% of these detected points are rejected in the standard PS approach without taking the azimuthal sub-pixel position into account.

For these rejected PS, we adapt the mathematical model (both functional and stochastic part) and iterated the PS estimation. Fig. 3a shows the result after iteration of the PS processing using the adopted functional model with azimuthal sub-pixel position. The density of PS did in this case not improve significantly (number of PS increased from 1749 to 1785 (2% improvement)). However, adding the sub-pixel position term in the stochastic model results in increased number of PS from 1749 to 1972 in deforming areas (Fig. 3b), that is 12% improvement in density of PS in the area of interest. These results show that it is better to deal with azimuthal sub-pixel position stochastically rather than functionally in this dataset.

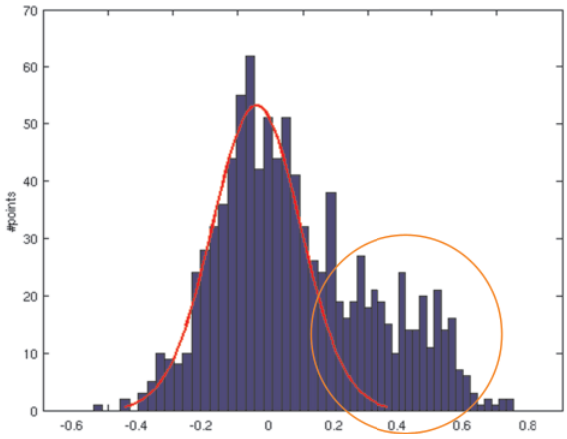

Figure 5. Histogram of correlation between residuals and Doppler differences.

7. FINAL RESULTS

After evaluating the three mentioned sources of type-I errors in the Gardanne area, we combined all proposed approaches together. That is, we applied the following adaption.

1. Adapted APS interpolation with trend and stratification effect.
2. Sequential hypothesis testing scheme using linear, breakpoint, and quaderatic models.
3. Iterative deformation modeling using kriging.
4. Adapted stochastic model for pixels with azimuthal sub-pixel position.

Fig. 4a shows the results. The density of PS in the deforming area increased significantly from 1749 to 2581, that is 48% improvement in PS detection capability. Fig. 4b presents the contribution of the different adaptions in PS density in the area of interest. Note that the sum of the three contribution (44%) is not equal to the total improvement (48%) due to the synergy effect among these optimizations. That is, integration of all these adaptions acting together improves the results more than applying the indivisual adaptions.

Improving the PS density in the deforming area results in better estimation of the final velocity map of the area. Figs. 6a and b show interpolated velocity maps using kriging interpolation for the standard PS approach and the adopted approach respectively. These results show that the adapted algorithm can better catch the deformation signal in this mining area.

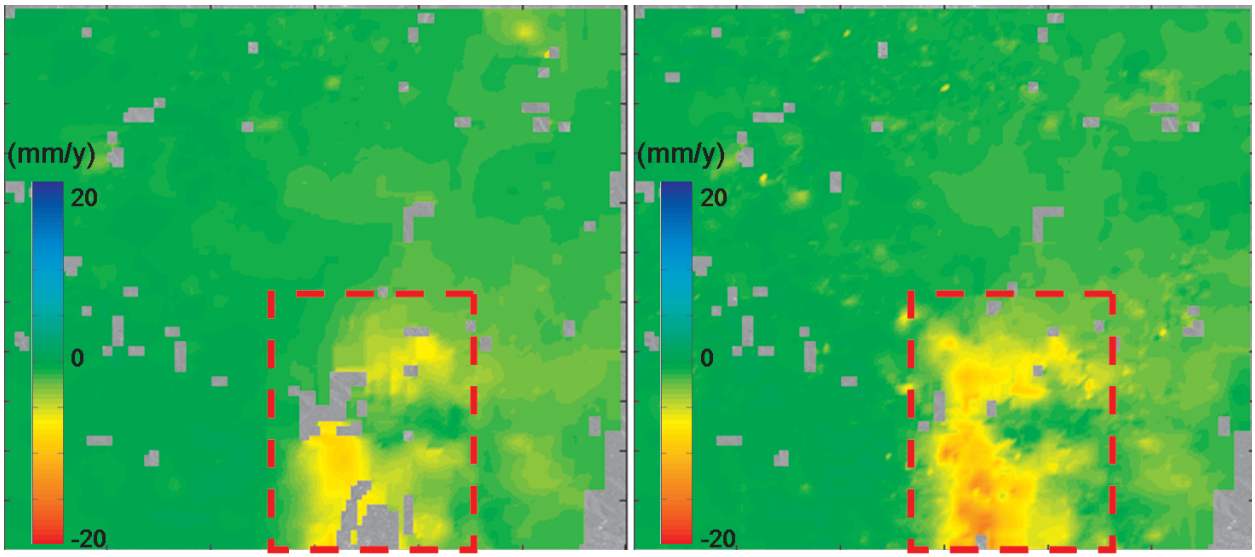

Figure 6. a) and b). Interpolated velocity maps using standard PS approach and adopted approach respectively.

8. CONCLUSIONS

The results of the PSIC4 study have been used to evaluate algorithm performance and assess which approaches are most important to retrieve reliable deformation parameters at a high spatial density. This includes an analysis of type-I errors (falsely rejected PS) due to imperfections in the functional model (e.g., imperfection due to non-linear deformation, sub-pixel position of the scatterer), or in the stochastic model (e.g. imperfection due to atmospheric errors, orbit errors, geometrical decorrelation). We investigate the contribution of three different sources of type I errors: atmosphere phase screen (APS) and orbital error, non-linear deformation mechanism, and azimuthal sub-pixel position of the scatterers and optimized the mathematical model to deal with these errors. The results show significant improvements in the identification of these type I errors, leading to improved PS density in the deforming area. Application of the proposed optimizations shows a 48% increase in the number of detected PS in the deforming area. This improvement can significantly improve the final velocity map which is one of the main products of the PSI technique from an application point of view.

REFERENCES

Ferretti, A., C. Prati, and F. Rocca (2001, January). Permanent scatterers in SAR interferometry. *IEEE Transactions on Geoscience and Remote Sensing 39*(1), 8–20.

Hanssen, R. F. (2001). *Radar Interferometry: Data Interpretation and Error Analysis*. Dordrecht: Kluwer Academic Publishers.

Kampes, B. M. (2005, September). *Displacement Parameter Estimation using Permanent Scatterer Interferometry*. Ph. D. thesis, Delft University of Technology, Delft, the Netherlands.

Kampes, B. M. and R. F. Hanssen (2004, November). Ambiguity resolution for permanent scatterer interferometry. *IEEE Transactions on Geoscience and Remote Sensing 42*(11), 2446–2453.

Marinkovic, P., G. Ketelaar, F. van Leijen, and R. Hanssen (2008). InSAR quality control: Analysis of five years of corner reflector time series. In *Fifth International Workshop on ERS/Envisat SAR Interferometry, 'FRINGE07', Frascati, Italy, 26 Nov-30 Nov 2007*, pp. 8 pp.

Racoules, D., B. Bourgine, M. de Michele, G. L. Cozannet, C. Luc, C. Bremmer, H. Veldkamp, D. Tragheim, L. Bateson, M. Crosetto, M. Agudo, and M. Engdahl (2006, June). Psic4: Persistent scatterer interferometry – independent validation and intercomparison of results. Technical report, BRGM. BRGM/RP-55640-FR.

Teunissen, P. J. G. and A. R. Amiri-Simkooei (2006). Least-squares variance component estimation. *Journal of Geodesy xx*, submitted.

van Leijen, F. J. and R. F. Hanssen (2007a). Persistent scatterer density improvement using adaptive deformation models. In *International Geoscience and Remote Sensing Symposium, Barcelona, Spain, 23–27 July 2007*, pp. 4 pp.

van Leijen, F. J. and R. F. Hanssen (2007b). Persistent scatterer interferometry using adaptive deformation models. In *ESA ENVISAT Symposium, Montreux, Switzerland, 23–27 April 2007*, pp. pp.